doi:10.2533/chimia.2022.546 Chimia 76 (2022) 546–551

Spectroscopic Tools to Investigate the Electrochemical Doping Kinetics and Efficiency in Organic Semiconductors

Olivier Bardagot and Natalie Banerji*

Abstract: Understanding the electrochemical doping of organic semiconductors plays a crucial role in the current development of organic electronics. In this short review, we present how temperature- and time-dependent visible-near-infrared (Vis-NIR) spectro-electrochemistry and terahertz spectroscopy, combined with multivariate curve resolution analysis, can inform on the fundamental mechanisms governing the doping kinetics and efficiency of two archetypal semiconducting polymers (PEDOT and P3HT). We highlight the experimental procedures and data analysis performed to access (i) the thermodynamic parameters driving the extent and dynamics of electrochemical reactions in doped systems and (ii) how the density and nature of charged species (polarons, bipolarons) impact the charge carrier delocalization, effective THz mobility and hence short-range conductivity.

Keywords: Doping kinetics · Electrochemistry · Terahertz conductivity · Mixed valence hopping transport

Olivier Bardagot is a post-doctoral researcher in Natalie Banerji's group at the University of Bern (2020–2022). He studied Physics Nanoscience at Grenoble INP and Imperial College London. He obtained his PhD in Polymer Science in 2019, under the supervision of Prof. Renaud Demadrille in SyMMES (France). His research focuses on developing functional and environmentally friendly organic devices by understanding the fundamental doping mechanisms that drive their performance.

Natalie Banerji is a Full Professor of Chemistry at the University of Bern. She is the leader of the FemtoMat group. Her research interests include the study of organic and hybrid materials using ultrafast spectroscopy, in view of bioelectronic and photovoltaic applications. She studied Chemistry at the University of Geneva and obtained her PhD in Physical Chemistry in 2009 (with Prof. Eric Vauthey). She studied organic photovoltaics during a post-doctoral stay (2009–2011) with Nobel Laureate Prof. Alan J. Heeger at the University of California in Santa Barbara, and consequently held independent positions at EPFL (Ambizione, 2011–2014) and at the University of Fribourg (Associate Professor, 2014–2017).

1. Introduction

The specific properties of organic semiconductors, compared to their inorganic counterparts, open the way to the development of new electronics with unique characteristics. To name a few, organic semiconductors such as π-conjugated polymers, allow flexible and more environmentally friendly thermogenerators for the conversion of heat losses into useful electricity,[1-2] high-capacitance electrodes for electrochemical energy storage,[3] or low cost and high sensitivity biosensors for healthcare applications.[4-5] These current device developments are promising and address current societal issues of alternative energy production and storage, as well as the increasing need for medical diagnostics and personalized treatments. However, in their intrinsic state, π-conjugated polymers typically have an electrical conductivity (σ) below 10^{-6} S cm^{-1}.[6] Consequently, doping – *i.e.*, the increase of the density of charge carriers – is required to reach the conductivities needed for the operation of these devices. Doping can be chemical (electron transfer due to the insertion of a dopant[7-8]) (Fig. 1a) or electrochemical (injection of a charge from an electrode to compensate for the insertion of an ion[9]) (Fig. 1b). The understanding of the fundamental mechanisms limiting the kinetics and efficiency of doping is hence paramount to afford educated molecular engineering and rational optimization of these technologies. In this article, we present how time-resolved visible-near-infrared (Vis-NIR) absorbance spectroscopy and *in situ* terahertz (THz) spectroscopy can provide insights on the mechanisms limiting the performance of chemically and electrochemically doped archetypal polymers such as poly(3,4-ethylenedioxythiophene):poly(styrenesulfonate) (PEDOT:PSS) and poly(3-hexylthiophene) (P3HT).

2. Temperature-dependent Vis-NIR Absorbance Spectro-Electrochemistry

To electrochemically dope an organic semiconductor, the material must be deposited onto a conductive electrode (working electrode) and immersed in an electrolyte together with, at least, one quasi-reference electrode (Fig. 1b).[10] By applying a voltage above the oxidation/reduction potential of the semiconductor between the working and the quasi-reference electrodes, one can control the doping extent.[11] Upon voltage application, solvated ions are driven inside the semiconductor matrix and an electronic charge carrier is injected from the working electrode to the semiconductor to ensure electroneutrality. The semiconductor undergoes electrochemical oxidation/reduction and its conductivity

*Correspondence: Prof. Dr. N. Banerji E-mail: natalie.banerji@unibe.ch Dept. of Chemistry, Biochemistry and Pharmaceutical Sciences, University of Bern, Freiestrasse 3, CH-3012 Bern, Switzerland

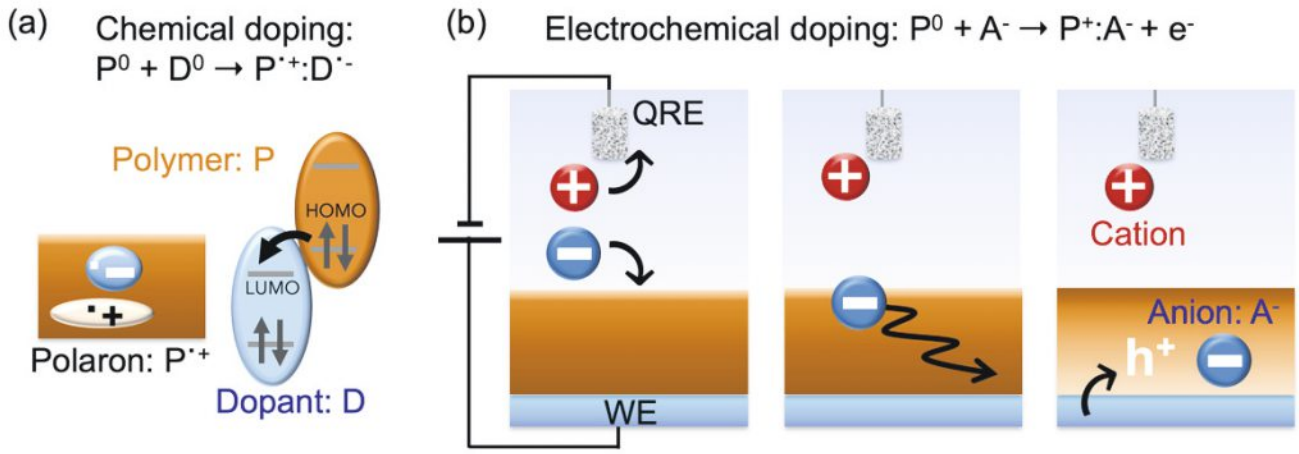

Fig. 1. (a) Schematic representation of chemical doping (ion-pair formation) and simplified energy level diagram illustrating electron transfer. P = semiconducting polymer, D = molecular dopant. (b) Schematic representation of the three main steps limiting the electrochemical doping kinetics of organic semiconductors, from left to right: electrolyte polarization, ion diffusion, oxidation/reduction of the semiconductor. A^- = anion, QRE = quasi-reference electrode, WE= working electrode.

changes. The dynamics of electrochemical doping of an organic semiconductor is mainly determined by three steps (Fig. 1b): (*i*) the electrolyte polarization (time for the positive and negative ions to form a double layer when voltage is applied), (*ii*) the ion diffusion (time for ions to travel through the semiconductor thickness), (*iii*) the oxidation/reduction of the semiconductor (time for charge carriers to be injected and induce the electrochemical reaction).[12]

First, the electrolyte polarization mainly depends on the ionic character of the salt (*i.e.*, its association energy),[13] its concentration (which influences the solvation degree)[14] and the distance between the two electrodes (*i.e.*, the electrolyte thickness).[15] Second, the ion diffusion is mainly limited by the semiconductor thickness[16] and the mobility of the ions within the semiconductor matrix. As a result, thicker films suffer more from ion-diffusion limitations that can be tempered by increasing film porosity.[17-18] If the solvated ions and the semiconductors are immiscible, ion penetration can be negligible, resulting in very limited doping extent only due to field-effect.[19-20] There are three main strategies to afford important and fast ion penetration. 1) Adapting the solvent of the electrolyte (polarity, viscosity). For instance, the use of ionic liquids fastens the doping kinetics, which can be further improved by dilution with acetonitrile.[21] 2)Modifying the nature of the ions (polarizability, size). For instance, aqueous KCl electrolyte essentially dopes P3HT only at the surface, while aqueous KPF_6 induces a large bulk doping effect.[22-23] 3) Engineering the structure of the semiconductor (side-chain engineering, film morphology).[22, 24-27] The substitution of apolar alkyl side chains by more polar oligo(ethylene glycol) side chains has proven to be an efficient strategy to increase doping efficiency and speed up doping kinetics.[28-30] Conversely, the addition of additives/co-solvents induces morphological changes that can impact the ion mobility. For instance, adding ethylene glycol in PEDOT:PSS casting solution causes a twofold decrease in ion mobility.[31] Lastly, the kinetics of the oxidation/reduction of the semiconductor depends on the energetics of the system, such as the energy barrier between the work function of the electrode and the HOMO/LUMO of the semiconductor that drives charge carrier injection,[32] and the thermodynamic parameters of the electrochemical reactions.

In the field of organic electronics, electrolyte polarization and ion diffusion are widely studied, but fundamentals driving electrochemical reactions are rarely investigated experimentally.

In our recent work, we combined temperature-dependent time-resolved Vis-NIR absorbance spectroscopy with kinetic modelling to address the thermodynamic parameters driving the kinetics of doping/dedoping of PEDOT:PSS films in NaCl aqueous electrolyte.[33]

Without applied voltage, PEDOT semiconducting polymer is intrinsically doped by the surrounding PSS^- ion-conductive matrix (Fig. 2a). Upon voltage application, one can control the injection of Na^+ to compensate the charge on PSS^- and dedope $PEDOT^{x+}$ to $PEDOT^0$.[31, 34] The experimental procedure to selectively assess the thermodynamic parameters driving the dedoping/redoping reactions is first to choose experimental conditions where electrolyte polarization and ion diffusion are not kinetically limiting. For PEDOT:PSS, we chose: 0.1 M electrolyte concentration, short electrode-film of thickness distance, thin film of ~ 100 nm. Then, the concentration of each species involved in the dedoping/redoping reactions must be evaluated. To do so, multivariate curve resolution (MCR) analysis can be used to decompose absorbance spectra into a convolution of (*i*) spectral signatures of the species of interest – here neutral species (N, no charge), polarons (P, paramagnetic, with unpaired spins) and bipolarons (B, diamagnetic, with paired spins) – and (*ii*) concentrations ([N], [P], [B]).[35] MCR analysis can be implemented from an open-source package on Python.[36] To first study what drives the successive electrochemical equilibria, steady-state absorbance spectra are acquired at different dedoping voltages. Analyzing the data with MCR provides the steady-state concentrations from which one can calculate the equilibrium constant using $K_{B \rightleftarrows P} = \ln([P]/[B])$ and $K_{P \rightleftarrows N} = \ln([N]/[P])$. Applying the same procedure for a range of temperatures (from 10ºC to 50ºC) allows to extract the temperature dependence of K and to estimate the enthalpy (ΔH_r) and entropy (ΔS_r) of reaction using the Van't Hoff equation (Fig. 2b).[37-38] For example, we found that the reduction of bipolarons to polarons and of polarons to neutral species is exothermic and thermodynamically favored at higher dedoping voltage and lower temperature.

Studying steady-state spectra provides insight on the equilibrium reactions that define the doping extent. Nonetheless, probing the reaction kinetics is equally important in view of optimizing applications relying on device time response such as neuromorphic[39-40] or electrophysiology devices.[41-42] Time-resolved absorbance spectroscopy upon application of voltage pulses is a fundamental tool to address reaction kinetics. We provide a description of a home-built instrument to perform such experiments in our previous work.[33] After MCR spectral decomposition of the obtained data, we observed that during dedoping, the bipolaron concentration promptly decays concomitantly with the rise of polarons (Fig. 2c). Only then, neutral species start to be formed, bipolarons reach complete depletion, while polarons reach a max-

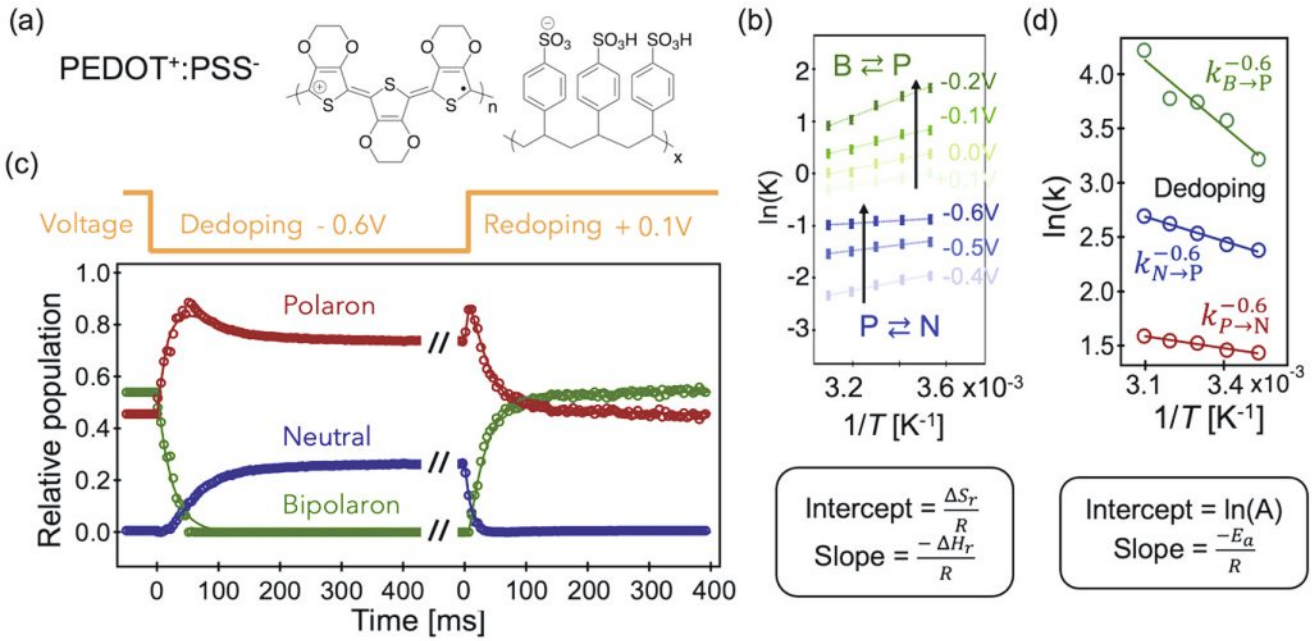

Fig. 2. (a) Chemical structure of PEDOT+:PSS-. (b) Van't Hoff plots obtained from temperature-dependent steady-state absorbance spectroscopy for the B ⇄ P equilibrium from +0.1 to –0.2 V versus Ag/AgCl and the P ⇄ N equilibrium from –0.4 to –0.6 V. The entropy (ΔSr) and enthalpy (ΔHr) of reaction are deduced from the intercept and slope, respectively. (c) Kinetic evolution of the neutral, polaron, and bipolaron populations for dedoping and redoping at 30°C (points = data, lines = fit from kinetic model). The rate constants k are deduced from the fits. (d) Arrhenius plots for the dedoping at -0.6 V versus Ag/AgCl. The activation entropy (ΔS‡) and enthalpy (ΔH‡) are deduced from the intercept and slope, using ΔS‡ = R x ln[Ah/(2.718 x k_BT)] and ΔH‡ = Ea - RT, respectively. Adapted from ref. [33].

imum. Later, polarons decay into neutral species and reach an equilibrium. Based on these observations, we built a kinetic model. The details of the hypotheses considered are described in our article.[33] The fit quality supports the finding that the dedoping occurs according to B → P ⇄ N, with the P ⇄ N equilibrium being rate limiting. A similar analysis led us to conclude that the redoping occurs in the reverse process N → P ⇄ B. One main benefit of building a kinetic model is to quantify the rate constants (k) of the oxidation/reduction reactions. In a similar fashion to the steady-state measurements, we repeated the time-resolved experiment at varying temperatures. Then, Arrhenius plots were used to access the pre-exponential factor A and activation energy E_a (Fig. 2d). Using the Eyring equation from transition state theory, one can then calculate the enthalpy (ΔH‡) and entropy (ΔS‡) of activation from A and E_a, respectively.[43] Note that these thermodynamic terms of *activation* define the changes from the initial state to the transition state. They differ from the terms of *reaction*, estimated from the equilibrium constant, that define the changes from the initial state to the final state (*i.e.*, reactant(s) to product(s)).

With these accessible tools and this experimental procedure, we provide a transferable way to access the thermodynamic parameters governing the extent and kinetics of the electrochemical doping of organic semiconductors. We found for PEDOT:PSS that dedoping is exothermic and enthalpy driven (charge destabilization when Na^+ compensate PSS^-). On the other hand, upon redoping, states are mainly stabilized by entropy (higher density of charge carriers and higher electronic delocalization). In both cases, we show that the reaction kinetics are mainly dominated by the entropy of activation with the redoping process being faster than the dedoping process. These results provide a new lens to further optimize electrochemical polymer doping and device operation.

3. Terahertz Spectroscopy

We have introduced temperature-dependent Vis-NIR absorbance spectroscopy to evaluate doping kinetics and doping extent. But interestingly, even if the charge carrier density increases upon chemical and electrochemical doping, the resulting enhancement of the macroscale conductivity is not directly proportional.[8, 44] The principal reasons are: (*i*) a charge carrier density threshold must be reached to offer percolation of conducting pathways,[45-46] (*ii*) even above this threshold, the induced charge carriers might not be mobile and may not contribute to transport,[47-48] (*iii*) the low doping efficiency of organic semiconductors requires to introduce several molar percent of dopants or ions that may disrupt the film morphology and increase energetic disorder,[49] and (*iv*) the transport properties of the mobile charge carriers vary upon doping due to changes in the microstructural and electrostatic environment.[50-51] Understanding the latter is of high interest from a fundamental point of view to guide molecular engineering and materials processing.

Concretely, the question is 'how does the density and nature (polarons, bipolarons) of the charged species impact the charge carrier delocalization and mobility?'. To answer it, we have proposed in our recent work to use THz spectroscopy.[52] THz spectroscopy probes the short-range transport properties of the doped conductive polymer. The length scale probed by THz spectroscopy ranges from tens to hundreds of nanometers, as it corresponds to the distance that a mobile charge carrier can travel within the electric field of a short THz pulse (~1 ps). As a result, THz spectroscopy enables us to disentangle the intrinsic transport properties of the doped material from the macroscale contributions (long-range disorder, grain boundaries, traps, and contact resistances). Note that this technique is only sensitive to charge carriers on the host semiconductor as the ones on the ions or ionized dopants are comparatively immobile due to higher localization.

In our recent study, we compare the short-range transport properties of P3HT upon electrochemical doping with 0.1 M aqueous KPF_6 or 0.1 M TBAPF6 in acetonitrile versus chemical doping with 17%mol 2,3,5,6-tetrafluor-7,7,8,8-tetracyan-chinodimethan (F_4TCNQ).[52] For *in situ* electrochemical measurements, a dedicated three-electrode cell was developed, and the film was

pre-cycled to stabilize the film morphology. THz spectra were acquired at steady state for different voltages. For doping voltages from –0.6 V to –1.0 V versus Ag/AgCl, a decay in amplitude and a phase shift of the transmitted THz electric field is observed (Fig. 3a). This results from an increase of the density of charge carriers that absorb and delay the THz pulses. After Fourier transformation of the transmitted time-domain THz electric field into the frequency domain, one can extract the refractive index (*n*) and absorption coefficient (*k*).[53-54] Knowing n(ω) and k(ω), the complex conductivity ($\tilde{\sigma}(\omega) = \sigma_{real} + i\sigma_{im}$, Fig. 3b) is calculated using the equations:

$$\sigma_{real}(\omega) = 2\omega\varepsilon_0\, n(\omega)k(\omega)$$
$$\sigma_{im}(\omega) = \omega\, \varepsilon_0\, (k^2(\omega) - n^2(\omega) + \varepsilon_{inf}) \quad (1)$$

where ε_0 is the vacuum permittivity and ε_{inf} the optical dielectric constant.

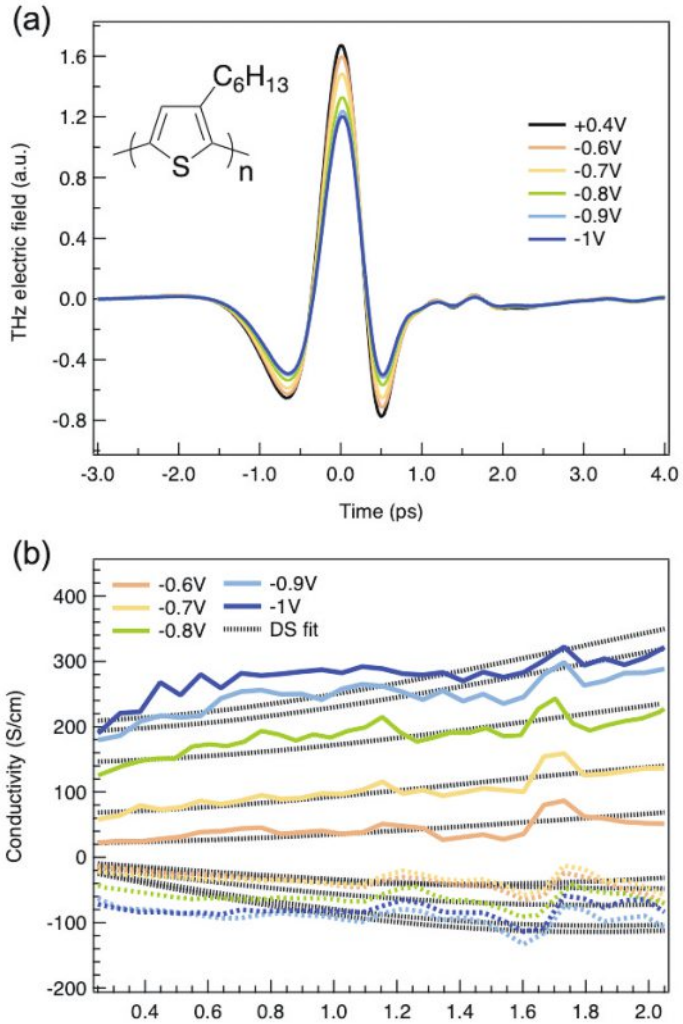

Fig. 3. (a) Transmitted time-domain THz electric field and (b) corresponding complex conductivity of electrochemically doped P3HT with aqueous KPF_6. The real and imaginary parts are shown as solid and dashed color lines, respectively. Drude-Smith (DS) fits are shown as black dashed lines. Inset: Chemical structure of P3HT. Adapted from ref. [52].

To quantify the effective THz mobility, the complex conductivity is then fitted with the phenomenological Drude-Smith model:

$$\tilde{\sigma}(\omega) = \frac{\varepsilon_0 \omega_P^2 \tau}{(1 - i\omega\tau)}\left[1 + \frac{c_1}{1 - i\omega\tau}\right] \quad (2)$$

The fit parameters are: the scattering time τ, the plasma frequency ω^P and the localization parameter c_1. Note that the scattering time τ was linked at all voltages as the real parts have similar shapes. Hypothesis made are detailed in our article.[52] Finally, the effective THz mobility (Fig 4) is obtained from:

$$\mu_{eff} = e\frac{\tau}{m^*}(1 + c_1) \quad (3)$$

with m* the effective mass assumed to be 1.7 m_e, m_e being the electron mass.[55]

The results are summarized in Fig. 4. First, we confirm that the effective mobility depends on the doping extent. It rises from –0.6 to –0.7 V up to ~7 $cm^2\ V^{-1}\ s^{-1}$ as the localization parameter c_1 becomes less negative (–0.91 to –0.78), and then stays constant at higher doping voltages. In parallel, the contributions of polarons and bipolarons were accessed as discussed above using steady-state absorbance spectro-electrochemistry and MCR analysis. From –0.6 to –0.7 V, the density of polarons remains constant while bipolarons increase. At higher voltages, more bipolarons are formed, but the effective mobility stagnates. The initial improvement in the effective mobility is thus not due to bipolarons being more conductive than polarons but can rather be assigned to the co-existence of polarons and bipolarons enabling mixed valence hopping transport. The decrease of the conductivity reported at very high doping extent when polarons are depleting supports the hypothesis that both polarons and bipolarons are required for efficient transport in doped P3HT.[52, 56]

Knowing that the effective mobility stagnates at higher doping levels, the continuous increase observed in the short-range conductivity is solely attributed to the increase of charge carrier density (Fig. 4). The difference between the injected carriers obtained *via* chronoamperometry (orange line), and the carrier density estimated from the Drude-Smith fits suggests that not all charge carriers are mobile enough to contribute to the transport. Overall, a maximal short-range conductivity of ~300 S cm^{-1} is obtained in aqueous KPF_6. By repeating this measurement in $TBAPF_6$/acetonitrile, we found ~270 S cm^{-1}, while a maximal macroscopic conductivity of 224 S cm^{-1} is reported in literature for electrochemically doped P3HT in the same electrolyte.[56] This difference indicates that the long-range losses and device structure cause a decrease of 20% in P3HT conductivity. In comparison, the maximal macroscopic conductivity obtained *via* chemical doping with F_4TCNQ is ~1.8 S cm^{-1} at 17%mol.[57] This dopant concentration (17 %mol) corresponds to a similar doping level reached at –0.6 V upon electrochemically doping, being associated to a short-range conductivity of ~36 S cm^{-1}.[52] The twentyfold difference is partly explained by an effective mobility one order of magnitude lower in the chemically doped system (Fig. 4). We attribute the lower mobility of the charges induced by chemical doping to the aggregation of ionized dopants and polymer chains, thereby causing higher static energetic disorder.[58] Note that at such high doping extent, Coulomb trapping has a negligeable effect compared to energetic disorder in the transport properties of doped organic semiconductors.[59]

4. Conclusions

In this work, we present two spectroscopic tools to gain insights on fundamental parameters that govern the kinetics and efficiency of doping in semiconducting polymers. Temperature-dependent Vis-NIR absorbance spectroscopy combined with computational MCR analysis and kinetic modelling allow to quantify the thermodynamic parameters controlling the electrochemical reactions of PEDOT:PSS thin film upon voltage application in aqueous NaCl electrolyte. After electrolyte polarization and ion diffusion

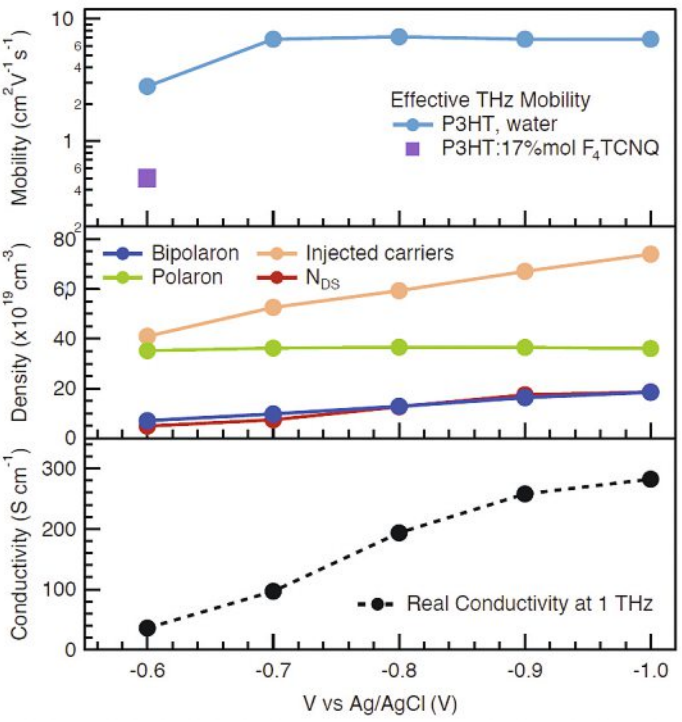

Fig. 4. Evolution of (top) the effective THz mobility, (middle) the injected charge carrier density extracted from chronoamperometry, the density of the polarons and bipolarons (from spectro-electrochemistry and MCR analysis) and the density of conductive charges from the Drude-Smith fits (N_{DS}, red line), and (bottom), the resulting real conductivity at 1 THz upon electrochemical doping of P3HT with aqueous KPF_6. Reproduced from ref. [52].

management, rational control of the enthalpy and entropy of the system *via* molecular engineering, morphological characterization, and theoretical calculations, is foreseen to be the challenge to address to further enhance the performance of electrochemical organic devices and extend their fields of application.

Complementarily, THz spectroscopy provides insights on the short-range conductivity and effective mobility induced upon doping. We learned that the co-existence of polarons and bipolarons affords a higher charge carrier delocalization in P3HT, which translates into a higher effective mobility in the electrochemical system. At high doping voltages, the rise in conductivity is only attributed to the increase in charge carrier density. THz spectroscopy is also a useful tool to compare the efficiency of different doping methods. We hence demonstrated that a higher conductivity could be reached *via* electrochemical doping and that at similar doping level, electrochemical doping induces more mobile charges than chemical doping in P3HT.

We believe that broadening the scope of materials and doping methods studied with these spectroscopic tools will deepen the understanding of the fundamental mechanisms driving doped organic devices and will provide important guidelines to rationally optimize future generations of organic semiconductors.

Acknowledgements:

The authors thank the European Commission for supporting this work by a European Research Council (ERC) Starting Grant (No. 714586, OSIRIS) and acknowledge NCCR-MUST, a research instrument of the Swiss National Science Foundation, as well as the University of Bern. The authors also thank Gonzague Rebetez and Dr. Demetra Tsokkou for proof-reading the manuscript.

Received: May 16, 2022

[1] T. A. Yemata, A. K. K. Kyaw, Y. Zheng, X. Wang, Q. Zhu, W. S. Chin, J. Xu, *Polym. Int.* **2020**, *69*, 84, https://doi.org/10.1002/pi.5921.
[2] S. Masoumi, S. O'Shaughnessy, A. Pakdel, *Nano Energy* **2022**, *92*, 106774, https://doi.org/10.1016/j.nanoen.2021.106774.
[3] M. G. Sumdani, M. R. Islam, A. N. A. Yahaya, S. I.Safie, *Polym. Eng. Sci.* **2022**, *62*, 269, https://doi.org/10.1002/pen.25859.
[4] L. Wang, X. Yue, Q. Sun, L. Zhang, G. Ren, G. Lu, H.-D. Yu, W. Huang, *Nano Res.* **2021**, *15*, https://doi.org/10.1007/s12274-021-3856-3.
[5] J. H. Kim, S. M. Kim, G. Kim, M. H. Yoon, *Macromol. Biosci.* **2020**, *20*, 2000211, https://doi.org/10.1002/mabi.202000211.
[6] T. Nunes Domschke, O. Bardagot, A. Benayad, R.Demadrille, A. Carella, R. Clerc, A. Pereira, *Synth. Met.* **2020**, 260, 116251, https://doi.org/10.1016/j.synthmet.2019.116251.
[7] J. Li, I. Duchemin, O. M. Roscioni, P. Friederich, M.Anderson, E. Da Como, G. Kociok-Köhn, W. Wenzel, C. Zannoni, D. Beljonne, X. Blase, G. D'Avino, *Mater. Horiz.* **2019**, *6*, 107, https://doi.org/10.1039/C8MH00921J.
[8] I. Salzmann, G. Heimel, M. Oehzelt, S. Winkler, N. Koch, *Acc. Chem. Res.* **2016**, *49*, 370, https://doi.org/10.1021/acs.accounts.5b00438.
[9] M. Modestov, V. Bychkov, D. Valiev, M. Marklund, *J. Phys. Chem. C* **2011**, *115*, 21915, https://doi.org/10.1021/jp205415y.
[10] N. Elgrishi, K. J. Rountree, B. D. McCarthy, E. S. Rountree, T. T. Eisenhart, J. L. Dempsey, *J. Chem. Educ.* **2018**, *95*, 197, https://doi.org/10.1021/acs.jchemed.7b00361.
[11] B. D. Paulsen, S. Fabiano, J. Rivnay, *Annu. Rev. Mater. Res.* **2021**, *51*, 73, https://doi.org/10.1146/annurev-matsci-080619-101319.
[12] P. Shiri, D. Neusser, C. Malacrida, S. Ludwigs, L. G. Kaake, *J. Phys. Chem. C* **2021**, *125*, 536, https://doi.org/10.1021/acs.jpcc.0c09527.
[13] R. Tao, X. Bi, S. Li, Y. Yao, F. Wu, Q. Wang, C. Zhang, J. Lu, *ACS Appl. Mater. Interfaces* **2017**, *9*, 7003, https://doi.org/10.1021/acsami.6b13859.
[14] A. Savva, C. Cendra, A. Giugni, B. Torre, J. Surgailis, D. Ohayon, A. Giovannitti, I. McCulloch, E. Di Fabrizio, A. Salleo, J. Rivnay, S. Inal, *Chem. Mater.* **2019**, *31*, 927, https://doi.org/10.1021/acs.chemmater.8b04335.
[15] D. A. Koutsouras, M. H. Amiri, P. W. M. Blom, F. Torricelli, K. Asadi, P. Gkoupidenis, *Adv. Funct. Mater.* **2021**, *31*, 2011013, https://doi.org/10.1002/adfm.202011013.
[16] P. Shiri, E. J. S. Dacanay, B. Hagen, L. G. Kaake, *J. Mater. Chem. C* **2019**, *7*, 12935, https://doi.org/10.1039/C9TC02563D.
[17] L. Huang, Z. Wang, J. Chen, B. Wang, Y. Chen, W. Huang, L. Chi, T. J. Marks, A. Facchetti, *Adv. Mater.* **2021**, *33*, 2007041, https://doi.org/10.1002/adma.202007041.
[18] R. Giridharagopal, J. Guo, J. Kong, D. S. Ginger, *ACS Appl. Mater. Interfaces* **2021**, *13*, 34616, https://doi.org/10.1021/acsami.1c08176.
[19] E. Zeglio, O. Inganäs, *Adv. Mater.* **2018**, *30*, 1800941, https://doi.org/10.1002/adma.201800941.
[20] J. Le Gall, F. Mouillard, T. N. Le, T. T. Vu, G. Mattana, R. Brayner, S. Zrig, V. Noël, B. Piro, *Biosens. Bioelectron.* **2020**, *157*, 112166, https://doi.org/10.1016/j.bios.2020.112166.
[21] W. Zhao, S. Bi, C. Zhang, P. D. Rack, G. Feng, *ACS Appl. Mater. Interfaces* **2019**, *11*, 13822, https://doi.org/10.1021/acsami.9b03433.
[22] L. Q. Flagg, R. Giridharagopal, J. Guo, D. S. Ginger, *Chem. Mater.* **2018**, *30*, 5380, https://doi.org/10.1021/acs.chemmater.8b02220.
[23] K. Melzer, M. Brändlein, B. Popescu, D. Popescu, P. Lugli, G. Scarpa, *Faraday Discuss.* **2014**, *174*, 399, https://doi.org/10.1039/C4FD00095A.
[24] Y. He, N. A. Kukhta, A. Marks, C. K. Luscombe, *J. Mater. Chem. C* **2022**, *10*, 2314, https://doi.org/10.1039/D1TC05229B.
[25] A. Savva, R. Hallani, C. Cendra, J. Surgailis, T. C. Hidalgo, S. Wustoni, R. Sheelamanthula, X. Chen, M. Kirkus, A. Giovannitti, A. Salleo, I. McCulloch, S. Inal, *Adv. Funct. Mater.* **2020**, *30*, 1907657, https://doi.org/10.1002/adfm.201907657.
[26] H. Toss, C. Suspène, B. Piro, A. Yassar, X. Crispin, L. Kergoat, M.-C. Pham, M. Berggren, *Org. Electron.* **2014**, 15, 2420, https://doi.org/10.1016/j.orgel.2014.06.017.
[27] G. Garcia-Belmonte, *Electrochem. Commun.* **2003**, *5*, 236, https://doi.org/10.1016/S1388-2481(03)00037-7.
[28] L. Q. Flagg, C. G. Bischak, J. W. Onorato, R. B. Rashid, C. K. Luscombe, D. S. Ginger, *J. Am. Chem. Soc.* **2019**, *141*, 4345, https://doi.org/10.1021/jacs.8b12640.
[29] P. A. Finn, I. E. Jacobs, J. Armitage, R. Wu, B. D. Paulsen, M. Freeley, M. Palma, J. Rivnay, H. Sirringhaus, C. B. Nielsen, *J. Mater. Chem. C* **2020**, *8*, 16216, https://doi.org/10.1039/D0TC04290K.
[30] B. Meng, J. Liu, L. Wang, *Polym. Chem.* **2020**, *11*, 1261, https://doi.org/10.1039/C9PY01469A.
[31] J. Rivnay, S. Inal, B. A. Collins, M. Sessolo, E. Stavrinidou, X. Strakosas, C. Tassone, D. M. Delongchamp, G. G. Malliaras, *Nat. Commun.* **2016**, *7*, 11287, https://doi.org/10.1038/ncomms11287.
[32] J.-H. Lee, J.-J. Kim, *Phys. Status Solidi A* **2012**, *209*, 1399, https://doi.org/10.1002/pssa.201228199.
[33] G. Rebetez, O. Bardagot, J. Affolter, J. Réhault, N. Banerji, *Adv. Funct. Mater.* **2022**, *32*, 2105821, https://doi.org/10.1002/adfm.202105821.
[34] P. Romele, M. Ghittorelli, Z. M. Kovács-Vajna, F. Torricelli, *Nat. Commun.* **2019**, *10*, https://doi.org/10.1038/s41467-019-11073-4.

[35] I. Zozoulenko, A. Singh, S. K. Singh, V. Gueskine, X. Crispin, M. Berggren, *ACS Appl. Polym. Mater*. **2019**, *1*, 83, https://doi.org/10.1021/acsapm.8b00061.
[36] C. H. Camp, Jr., *J. Res. Natl. Inst. Stand. Technol*. **2019**, *124*, 1, https://doi.org/10.6028/jres.124.018.
[37] S. Ogi, V. Stepanenko, K. Sugiyasu, M. Takeuchi, F. Würthner, *J. Am. Chem. Soc*. **2015**, *137*, 3300, https://doi.org/10.1021/ja511952c.
[38] N. Denderz, J. Lehotay, *J. Chromatogr. A* **2012,** *1268*, 44, https://doi.org/10.1016/j.chroma.2012.10.025.
[39] S. Yamamoto, G. G. Malliaras, *ACS Appl. Electron. Mater*. **2020**, *2*, 2224, https://doi.org/10.1021/acsaelm.0c00203.
[40] P. Zhao, R. Ji, J. Lao, W. Xu, C. Jiang, C. Luo, H. Lin, H. Peng, C.-G. Duan, *Org. Electron*. **2022**, *100*, 106390, https://doi.org/10.1016/j.orgel.2021.106390.
[41] W. Lee, D. Kim, J. Rivnay, N. Matsuhisa, T. Lonjaret, T. Yokota, H. Yawo, M. Sekino, G. G. Malliaras, T. Someya, *Adv. Mater*. **2016**, *28*, 9722, https://doi.org/10.1002/adma.201602237.
[42] S. Bontapalle, M. Na, H. Park, K. Sim, *Chem. Commun*. **2022**, *58*, 1298, https://doi.org/10.1039/D1CC04884H.
[43] S. Jhulki, H.-I. Un, Y.-F. Ding, C. Risko, S. K. Mohapatra, J. Pei, S. Barlow, S. R. Marder, *Chem.* **2021**, *7*, 1050, https://doi.org/10.1016/j.chempr.2021.01.020.
[44] B. D. Paulsen, C. D. Frisbie, *J. Phys. Chem. C* **2012**, *116*, 3132, https://doi.org/10.1021/jp2093934.
[45] S. Goffri, C. Müller, N. Stingelin-Stutzmann, D. W. Breiby, C. P. Radano, J. W. Andreasen, R. Thompson, R. A. J. Janssen, M. M. Nielsen, P. Smith, H. Sirringhaus, *Nat. Mater*. **2006**, *5*, 950, https://doi.org/10.1038/nmat1779.
[46] C. Francis, D. Fazzi, S. B. Grimm, F. Paulus, S. Beck, S. Hillebrandt, A. Pucci, J. Zaumseil, *J. Mater. Chem. C* **2017**, *5*, 6176, https://doi.org/10.1039/C7TC01277B.
[47] A. Higgins, S. K. Mohapatra, S. Barlow, S. R. Marder, A. Kahn, *Appl. Phys. Lett*. **2015**, *106*, 163301, https://doi.org/10.1063/1.4918627.
[48] A. Karki, G. J. A. H. Wetzelaer, G. N. M. Reddy, V.Nádaždy, M. Seifrid, F. Schauer, G. C. Bazan, B. F. Chmelka, P. W. M. Blom, T. Q. Nguyen, *Adv. Funct. Mater*. **2019**, *29*, 1901109, https://doi.org/10.1002/adfm.201901109.
[49] R. A. Schlitz, F. G. Brunetti, A. M. Glaudell, P. L. Miller, M. A. Brady, C. J. Takacs, C. J. Hawker, M. L. Chabinyc, *Adv. Mater.* **2014**, *26*, 2825, https://doi.org/10.1002/adma.201304866.
[50] I. Enokida, Y. Furukawa, *Chem. Lett*. **2019**, *48*, 498, https://doi.org/10.1246/cl.190039.
[51] E. M. Thomas, M. A. Brady, H. Nakayama, B. C. Popere, R. A. Segalman, M. L. Chabinyc, *Adv. Funct. Mater*. **2018**, *28*, 1803687, https://doi.org/10.1002/adfm.201803687.
[52] D. Tsokkou, P. Cavassin, G. Rebetez, N. Banerji, *Mater. Horiz.* **2022**, *9*, 482, https://doi.org/10.1039/D1MH01343B.
[53] J. Neu, C. A. Schmuttenmaer, *J. Appl. Phys*. **2018,** *124*, 231101, https://doi.org/10.1063/1.5047659.
[54] D.-X. Zhou, E. P. J. Parrott, D. J. Paul, J. A. Zeitler, *J. Appl. Phys*. **2008**, *104*, 053110, https://doi.org/10.1063/1.2970161.
[55] J. E. Northrup, *Phys. Rev. B* **2007**, *76*, https://doi.org/10.1103/PhysRevB.76.245202.
[56] D. Neusser, C. Malacrida, M. Kern, Y. M. Gross, J. Van Slageren, S. Ludwigs, *Chem. Mater*. **2020**, *32*, 6003, https://doi.org/10.1021/acs.chemmater.0c01293.
[57] D. T. Duong, C. Wang, E. Antono, M. F. Toney, A. Salleo, *Org. Electron*. **2013**, *14*, 1330, https://doi.org/10.1016/j.orgel.2013.02.028.
[58] I. E. Jacobs, E. W. Aasen, J. L. Oliveira, T. N. Fonseca, J. D. Roehling, J. Li, G. Zhang, M. P. Augustine, M. Mascal, A. J. Moulé, *J. Mater. Chem. C* **2016**, *4*, 3454, https://doi.org/10.1039/C5TC04207K.
[59] I. E. Jacobs, G. D'Avino, V. Lemaur, Y. Lin, Y. Huang, C. Chen, T. F. Harrelson, W. Wood, L. J. Spalek, T. Mustafa, C. A. O'Keefe, X. Ren, D. Simatos, D. Tjhe, M. Statz, J. W. Strzalka, J.-K. Lee, I. McCulloch, S. Fratini, D. Beljonne, H. Sirringhaus, *J. Am. Chem. Soc*. **2022**, *144*, 3005, https://doi.org/10.1021/jacs.1c10651.